

Short Communication

## Influence of Thermally Sprayed WC-Co-Cr Coatings on the Corrosion Characteristics of Ni-Al Bronze Alloy

Luda Lee, Sunjung Kim\*

School of Materials Science and Engineering, University of Ulsan, Ulsan 44610, Republic of Korea

\*E-mail: [sunjungkim@ulsan.ac.kr](mailto:sunjungkim@ulsan.ac.kr)

Received: 26 February 2020 / Accepted: 8 April 2021 / Published: 31 May 2021

WC-Co-Cr coatings were thermally sprayed onto a Ni-Al bronze (NAB) alloy using the high velocity oxy-fuel (HVOF) process in order to increase the corrosion resistance of the NAB alloy, which is widely used for ship propellers operating in seawater. The superior corrosion resistance of the WC-Co-Cr coated NAB alloy, relative to the uncoated NAB alloy, was demonstrated by plotting their potentiodynamic polarization curves and conducting 80-day duration immersion tests in a 3.5% NaCl solution. The anti-corrosive properties of the WC-Co-Cr coated NAB alloy were improved by shortening spray distances and increasing hydrogen flow rates in the HVOF process.

**Keywords:** Corrosion; Ni-Al bronze alloy; Tungsten carbide coating; Binder

### 1. INTRODUCTION

A screw propeller is, with the body and engine, one of three main components of a ship. Screw propellers of ships significantly influence the headway, vibration, noise, and fuel consumption of ships in operation. When a ship operates in a marine environment, the fatigue phenomenon induced by high-speed cyclic movement of the propeller and the highly corrosive seawater environment decrease the lifetime of the propeller considerably. In addition, cavitation, which occurs around the blades of propellers, can cause a serious decline in propulsion efficiency and result in mechanical damage to the propeller [1]. In consideration of the harsh environments in which propellers operate, nickel-aluminum bronze (NAB) alloy, which is highly resistive to cavitation and corrosion, has been used for ship propellers, especially those operating in seawater [2,3].

NAB alloy has some disadvantages for use in ship propellers. Fabrication costs for complicated shapes are very high; moreover, fatigue cracking can occur during operation, and excess noise may also be produced due to the low acoustic damping performance of the alloy. Nevertheless, NAB alloy propellers have replaced manganese-bronze alloy propellers because of their relatively high tensile

strength and excellent durability. In addition, NAB alloy propellers have shown superior anti-fouling, anti-corrosion, and stiffness properties under operation at high torque in seawater [4,5].

We concern on the further enhancement of NAB alloy in seawater by applying an anti-corrosion coating to the surface of the alloy. Anti-corrosion coatings applied to the surface of a ship propeller serve to retard the corrosion reaction, and, to some extent, to protect the propeller from mechanical damage during operation [6]. Furthermore, corrosion damage of NAB alloy propellers with anti-corrosion coating can be easily and inexpensively repaired by coating damaged surface locally. In this study, a thermal spray coating technology was employed to coat the NAB alloy with tungsten carbide-cobalt-chromium (WC-Co-Cr), in order to further increase the corrosion resistance of the NAB alloy. WC-Co-Cr powders with high hardness and toughness are thermally sprayed to form an anti-abrasive or anti-corrosive coating in some applications [7,8]. The thermal spray coating process is an eco-friendly surface treatment technology widely used in order to extend the lifetime of plants and parts in various industries [9]. Conventional thermal spray technology can produce a coating of uniform thickness using a variety of coating materials. However, the technology can produce compositionally inhomogeneous coatings and may result in poor adhesion between the base metal and the coating. In particular, the conventional thermal spray of WC-Co-Cr can result in the decarbonization of WC [10]. In an effort to overcome the limitations of the conventional thermal spray coating process, the high velocity oxy-fuel (HVOF) thermal spray coating process was employed in this study. The HVOF process can produce a highly dense WC-Co-Cr coating structure with good adhesion strength, low porosity, and high deposition efficiency by uniformly spraying molten WC-Co-Cr at extremely high velocity.

In this study, the corrosion characteristics of NAB alloy coated with WC-Co-Cr by the HVOF process are investigated in a 3.5% NaCl solution, simulating the environment of ship propellers operating in seawater. The comparative corrosion study is performed by changing the spray distance and the flow rate of hydrogen, which is required to melt WC-Co-Cr powders.

## 2. EXPERIMENTAL

### 2.1. Preparation of NAB alloy blocks

The NAB alloy was produced by smelting pure Cu, Ni, Fe, Al, and Mn ingots of 99.9% purity in a SiC crucible. Cu, Ni, and Fe were first charged into the crucible, which was heated to 1350 °C; Al and Mn were then added to the molten alloy. The alloying elements were mixed by stirring continuously with a graphite bar. The molten NAB alloy was poured into a graphite mold for cooling after being maintained at 1100 °C for 5 min. Solidified NAB alloy blocks underwent a multi-stage rolling process consisting of a 50% hot rolling, a 30% cold rolling, an intermediate annealing for 1 hr, and a 30% cold rolling. NAB alloy blocks with an elemental composition of 5% Ni-2% Mn-9% Al-4% Fe-Cu were fabricated finally. The NAB alloy blocks were cut into specimens with dimensions of 2 × 2 × 0.5 cm.

## 2.2. HVOF thermal spray of WC-Co-Cr coating

In order to simulate the surface polishing treatment of ship propeller blades in industry, the surfaces of the NAB alloy specimens were polished using 0.05- $\mu\text{m}$  alumina slurry in a grinder. A HVOF thermal spray device was used to apply the WC-Co-Cr coating to the surface of the NAB alloy specimen. The spray distance was defined as a horizontal distance between a spray nozzle tip and a specimen surface. Separate WC (Praxair), Co (Praxair), and Cr (Sigma-Aldrich) powders with 3- $\mu\text{m}$  diameter were mechanically blended within a zirconia jar (ZMP-05, Sungho), which was mounted on two roller bars of a ball mill (BML-6, Daihan) without charging grinding balls. Chemical composition of the mixed powder was 86 wt% WC, 10 wt% Co, and 4 wt% Cr. The spray velocity of the HVOF device was 800  $\text{m s}^{-1}$ , and the target thickness of the WC-Co-Cr coating was 200  $\mu\text{m}$ . Table 1 shows the process parameters of the HVOF thermal spray used in this study. The spray distance and the flow rate of hydrogen were the parameters permitted to vary, based on the expectation that they may affect the corrosion properties of the WC-10% Co-4% Cr (WC-10Co-4Cr) coated NAB alloy.

**Table 1.** Process parameters of HVOF thermal spray.

Specimen	Coating material	Oxygen ( $\text{l min}^{-1}$ )	H <sub>2</sub> flow rate ( $\text{l min}^{-1}$ )	Air ( $\text{l min}^{-1}$ )	Amount of coated powder (g)	Spray distance (mm)
H1	WC-10Co-4Cr	32	62	44	38	200
H2	WC-10Co-4Cr	32	62	44	38	230
H3	WC-10Co-4Cr	32	62	44	38	260
T1	WC-10Co-4Cr	32	55	44	38	230
T2	WC-10Co-4Cr	32	62	44	38	230
T3	WC-10Co-4Cr	32	70	44	38	230

## 2.3. Metallographic preparation and analysis of WC-Co-Cr coating

Surface microstructure of as-deposited WC-Co-Cr coatings was observed in order to figure out the change of their surface morphologies according to the HVOF process parameters using a field emission scanning electron microscope (FESEM; Quanta 200, FEI). SEM images of polished coating surface were also taken to view the arrangement and dispersion of WC particles and Co/Cr binder. In addition, the cross-sectional microstructure of WC-Co-Cr coated NAB alloy was imaged with the FESEM for the verification of interfacial delamination between coating and NAB alloy after adhesion strength test using a pull-off tester (Romulus, Quad Group). Interfacial adhesion strength of individual coating was measured five times, then was averaged. Porosity of the as-deposited coating was also the average of five measurements using a surface area porosity analyzer (Gemini VII 2390, Micromeritics).

#### 2.4. Electrochemical corrosion test

Potentiodynamic polarization curves of the uncoated NAB and WC-10Co-4Cr coated NAB alloys in a 3.5% NaCl solution of pH 7.7 were obtained using a potentiostat (IviumStat, Ivium Technology, Inc.). A platinum mesh was used as a counter electrode, and a saturated calomel electrode (SCE) as a reference electrode. Responsive current density for NAB alloy specimens with as-deposited coatings and uncoated NAB alloy specimen was recorded while potential was scanned at a rate of  $1 \text{ mV s}^{-1}$  in the range from -1.3 to 3.0 V vs SCE. Three polarization tests were conducted to assure the repeatability of corrosion characteristic for each coating condition. In addition, the immersion tests in the 3.5% NaCl solution were conducted for 80 days to facilitate optical observation of specimen corrosion. Only one side of the NAB alloy specimens was immersed in the NaCl solution; the specimens were mounted on 1-cm diameter rubber rings with circular cross-sections. We expect that crevice corrosion condition is formed near the rubber rings due to their cross-sectional morphology, such that a more corrosive environment is created locally on the surface of the NAB alloy specimen in contact with the rubber ring.

### 3. RESULTS AND DISCUSSION

#### 3.1. Microstructures of WC-Co-Cr coatings

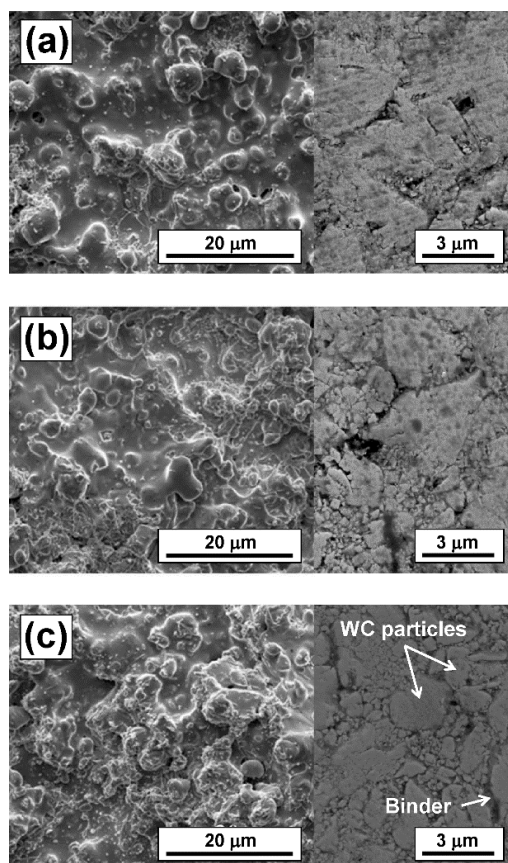


**Figure 1.** SEM images of microstructures of as-deposited (left) and polished (right) WC-10Co-4Cr coatings under varying HVOF spray distances [(a) 200 mm, (b) 230 mm, and (c) 260 mm].

Fig. 1 shows the microstructure of the WC-Co-Cr coating applied with a spray distance of 200, 230, and 260 mm, respectively. As the spray distance in the HVOF process increases, the WC particles become slightly smaller, because the particles experience more scattering events on the surface of the NAB alloy. Table 2 shows the chemical compositions of the WC-Co-Cr coatings as a function of the HVOF coating conditions. At longer spray distances, as Table 2 indicates an increase in Co and Cr content, spaces between WC particles are filled with more molten Co and Cr binder. Co and Cr are least corrosive in water by forming an oxide layer. Thus, the corrosion of WC-Co-Cr coatings could be governed by the extent of oxidation of WC particles [12,13]. However, for the WC-Co-Cr coating sprayed at longer distances, the oxide layer does not cover the coating surface continuously due to the existence of larger interfacial area between WC particles and binder. Takeda *et al.* reported previously that an incomplete coverage of a passive oxide layer on the surface of a thermally sprayed WC coating had a limited influence on corrosion characteristic [14-16].

**Table 2.** Chemical compositions of WC-Co-Cr coatings.

Specimen	C (wt%)	O (wt%)	W (wt%)	Cr (wt%)	Co (wt%)
H1	2.57	3.08	67.93	7.05	19.37
H2	2.43	4.04	64.25	8.52	20.76
H3	3.02	3.27	57.21	11.52	24.98
T1	2.78	3.35	61.20	11.76	20.91
T2	2.43	4.04	64.25	8.52	20.76
T3	1.61	4.20	60.88	10.07	23.24

Corrosion can occur considerably through the interfaces between WC particles and binder in a highly corrosive NaCl solution due to concentrated chlorine ions within the interfaces. At shorter spray distances, molten Co and Cr form a continuous oxide layer with covering the end surface of the coating entirely, as seen in as-deposited coating surfaces of Fig. 1. The adhesion strength of the WC-Co-Cr coating to NAB alloy is improved by spraying WC-Co-Cr powder at shorter distances because higher particle velocity could increase the surface temperature of NAB alloy. Therefore, it is expected that the NAB alloy coated with WC-Co-Cr at a shorter spray distance may tend to corrode less in the NaCl solution. On the other hand, as the hydrogen flow rate in the HVOF process increases, the enthalpy of heating WC, Co, and Cr powders increases. Thus, as shown in Fig. 2, higher hydrogen flow rates result in increased packing density of WC-Co-Cr structures, as well as increased strength of WC-Co-Cr adhesion to the NAB alloy. A previous study reported similarly that a higher hydrogen pressure could reduce the grain size of thermally sprayed WC-Co coatings, resulting in a denser microstructure [17,18].

### 3.2. Interfacial adhesion strength and porosity

We performed pull-off tests of WC-Co-Cr coated NAB alloys to measure interfacial adhesion

strength according to the spray distance and the hydrogen flow rate, as shown in Fig. 3. Lower porosity and better adhesion of the WC-Co-Cr coating would lead to improved corrosion resistance in the NaCl solution. Less porosity of thermally sprayed WC-Co-Cr coatings along with decreasing the spray distance or increasing the hydrogen flow rate was also reported previously [9,11]. Table 2 does not indicate a significant difference in chemical composition between specimens when changing hydrogen flow rate. A strong relationship between a porosity of thermally sprayed WC-Co coatings and a corrosion rate of diverse metal substrates can be supported by related previous reports, where metals HVOF-coated with WC-Co layers of lower porosity possess much improved resistance against various forms of corrosion in NaCl solutions [19-21].

In addition, it was previously suggested that the adhesion strength of HVOF-sprayed WC-Co-Cr coatings should be above 89 MPa in order to avoid an interfacial failure and corrosion damage under corrosive NaCl environment [22]. In Fig. 3 showing pull-off test results, H3 specimen with a spray distance of 260 mm and T1 specimen with a hydrogen flow rate of 55 l min<sup>-1</sup> did not reach the suggested criterion of adhesion strength. This relatively poor adhesion strength of H3 and T1 specimens resulted in more serious corrosion damage in comparison with other specimens, of which adhesion strength was over 100 MPa, as shown in Fig. 5.

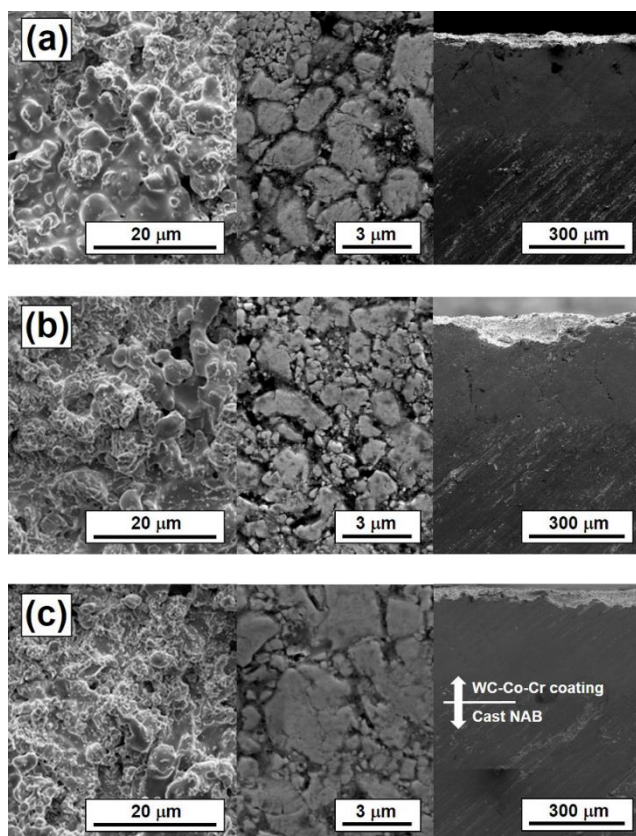


**Figure 2.** SEM images of microstructures of as-deposited (left) and polished (middle) WC-10Co-4Cr coating surface, and cross-sections (right) of WC-10Co-4Cr coated NAB alloys under varying hydrogen flow rates [(a) 55 l min<sup>-1</sup>, (b) 62 l min<sup>-1</sup>, and (c) 70 l min<sup>-1</sup>].

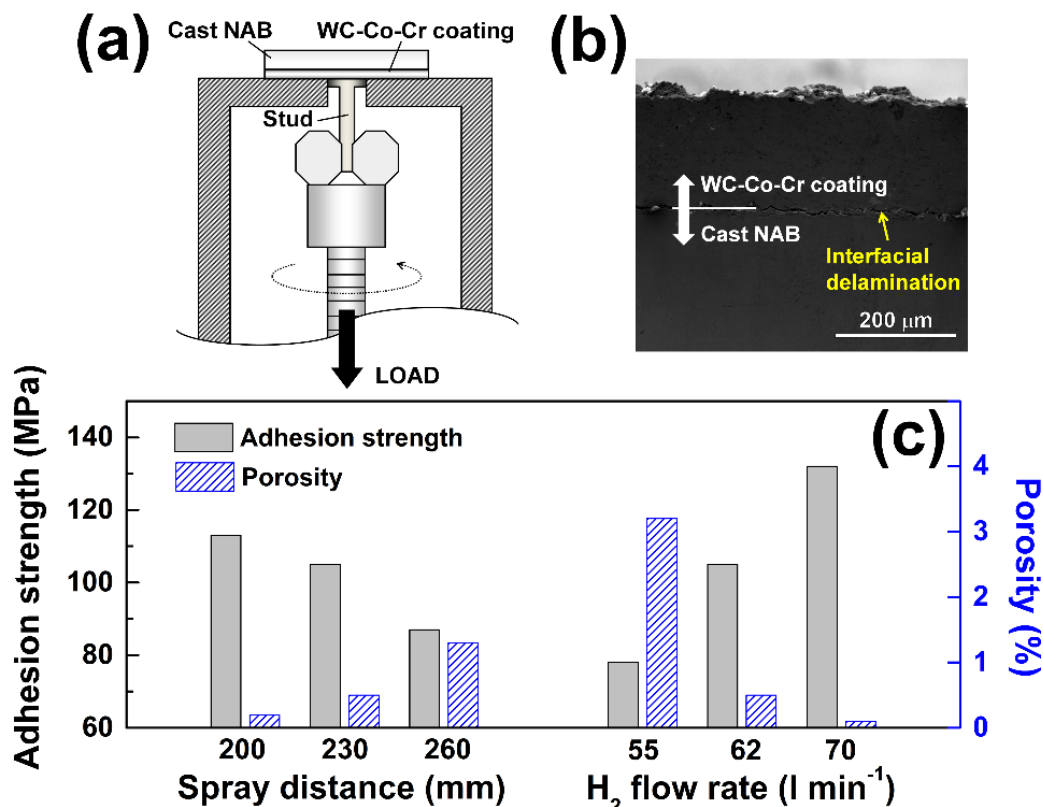


**Figure 3.** (a) schematic diagram of an apparatus for pull-off adhesion test, in which tensile stress was applied up to 200 MPa, (b) a cross-sectional SEM image showing the interfacial delamination between WC-10Co-4Cr coating and NAB alloy, and (c) the variation of both adhesion strength and porosity as for the spray distance (200, 230, and 260 mm) and hydrogen flow rate (55, 62, and 70 l min<sup>-1</sup>).

### 3.3. Corrosion characteristics

Fig. 4 shows the potentiodynamic polarization curves of WC-Co-Cr coated NAB alloys in NaCl solution under variation of conditions of the HVOF process. The curves are plotted along with that of the uncoated NAB alloy. Fig. 4a shows that the behavior of the polarization curves depends on the spray distance. The difference in corrosion potential and in corrosion current density between the WC-Co-Cr coated NAB alloys and the uncoated NAB alloy is insignificant. However, as the applied potential enters the anodic region, the corrosion rate of the uncoated NAB alloy becomes larger by over two orders of magnitude than that of the WC-Co-Cr coated NAB alloys. At more highly anodic potentials, the uncoated NAB alloy is passivated up to 2 V. The WC-Co-Cr coated NAB alloys show a different behavior of polarization according to the spray distance. The increase in the corrosion rate of the H1 specimen coated at a shorter distance is less sharp than that of the H2 and H3 specimens, indicating that the H1 specimen is less corrosive in the anodic region. The spray distance in the HVOF thermal spray process is known as the most important factor to determine the porosity and corrosion tendency of WC-Co-Cr coatings [23-25]. A shorter spray distance leads to a denser microstructure of the coating because the temperature of powder particles can be kept higher during thermal coating procedure on a substrate. Thus, the lowest porosity of H1 specimen, which was HVOF-coated at a

spray distance of 200 mm, concluded its highest resistance to corrosion in Fig. 4a.

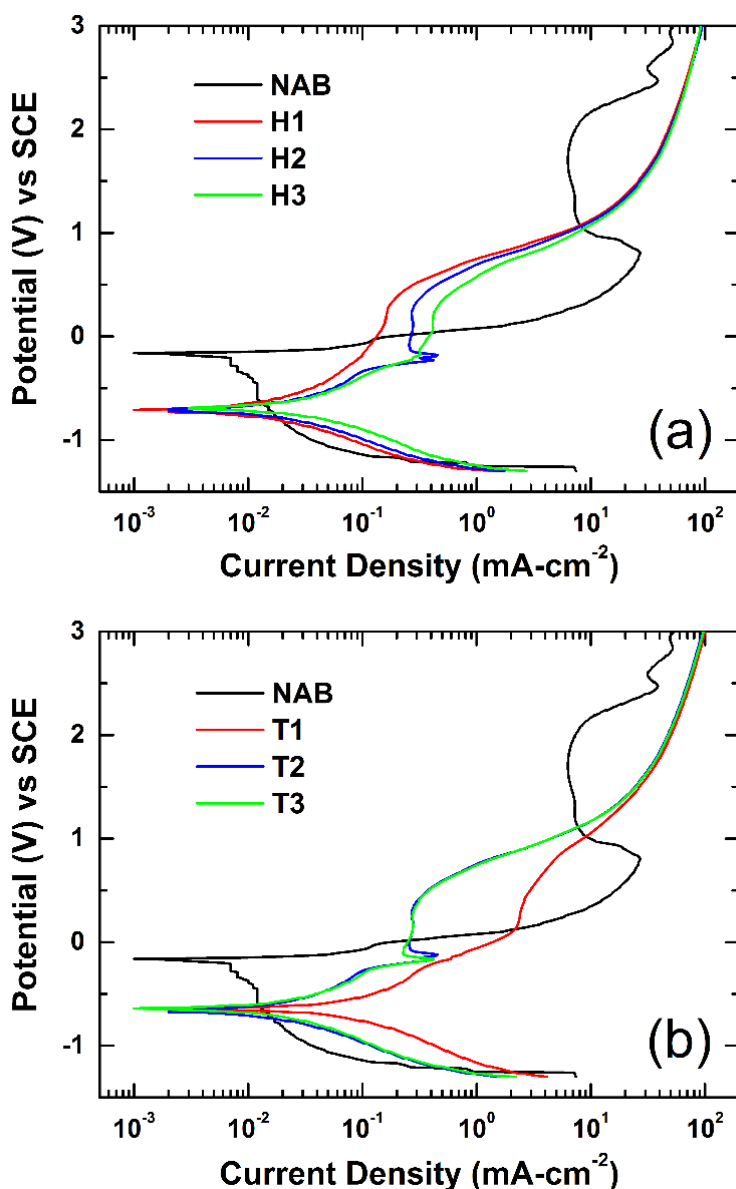


**Figure 4.** Potentiodynamic polarization curves of WC-10Co-4Cr coated NAB alloys in comparison with the uncoated NAB alloy (solid line) in a 3.5% NaCl solution. Potential was scanned at a rate of  $1 \text{ mV s}^{-1}$  in the range from  $-1.3$  to  $3.0 \text{ V vs SCE}$ . The applied spray distance was 200, 230, and 260 mm, respectively, for H1, H2, and H3 in (a). The hydrogen flow rate was 55, 62, and  $70 \text{ l min}^{-1}$ , respectively, for T1, T2, and T3 in (b).

Fig. 4b shows the variation in polarizing behavior of the WC-Co-Cr coated NAB alloys according to the hydrogen flow rate, in comparison with that of the uncoated NAB alloy. The corrosion rates of specimens T1 to T3 are much smaller than that of the uncoated NAB alloy at anodic potentials up to 1 V, similar to the cases of the H1 to H3 specimens. However, the T1 specimen coated at a lower hydrogen flow rate is slightly more corrosive than the T2 and T3 specimens in the anodic region. In

recent reports, it was proposed that higher hydrogen flow rates in the HVOF thermal spray of carbide-based coatings could affect positively the hardness and porosity of the coatings [26,27]. The structural rigidity of the coatings deposited at elevated hydrogen flow rates may describe the less corrosive behavior of T2 and T3 specimens coated at higher hydrogen flow rates. To summarize our observations from the polarization curves in Fig. 4, WC-Co-Cr coated NAB alloys are more resistant to corrosion in the NaCl solution than the uncoated NAB alloy in the region of moderate anodic potentials of interest. Moreover, the anti-corrosion characteristics of the WC-Co-Cr coated NAB alloys are slightly improved when the coating process is conducted using a shorter spray distance and a larger flow rate of hydrogen. Table 3 shows electrochemical corrosion parameters of WC-Co-Cr coated NAB alloys in comparison to the uncoated NAB alloy, which were acquired from the polarization curves of Fig. 4.

**Table 3.** Electrochemical corrosion parameters of each specimen in potentiodynamic polarization curves of Fig. 4.

Specimen	H <sub>2</sub> flow rate (l min <sup>-1</sup> )	Spray distance (mm)	Critical current density, <i>i<sub>critical</sub></i> (mA cm <sup>-2</sup> )	Passive current density, <i>i<sub>p</sub></i> (mA cm <sup>-2</sup> )	Redox Potential, <i>E<sub>redox</sub></i> (V)	Exchange current density, <i>i<sub>0</sub></i> (mA cm <sup>-2</sup> )
NAB	N/A	N/A	26.79	6.18	-0.16	4.9 × 10 <sup>-2</sup>
H1	62	200	N/A	0.17	-0.67	1.3 × 10 <sup>-2</sup>
H2	62	230	0.45	0.27	-0.66	9.2 × 10 <sup>-3</sup>
H3	62	260	N/A	0.42	-0.67	1.2 × 10 <sup>-2</sup>
T1	55	230	N/A	2.47	-0.64	2.9 × 10 <sup>-2</sup>
T2	62	230	0.45	0.27	-0.66	9.2 × 10 <sup>-3</sup>
T3	70	230	0.42	0.23	-0.64	6.4 × 10 <sup>-3</sup>

3.4. 80-day immersion test in NaCl solution

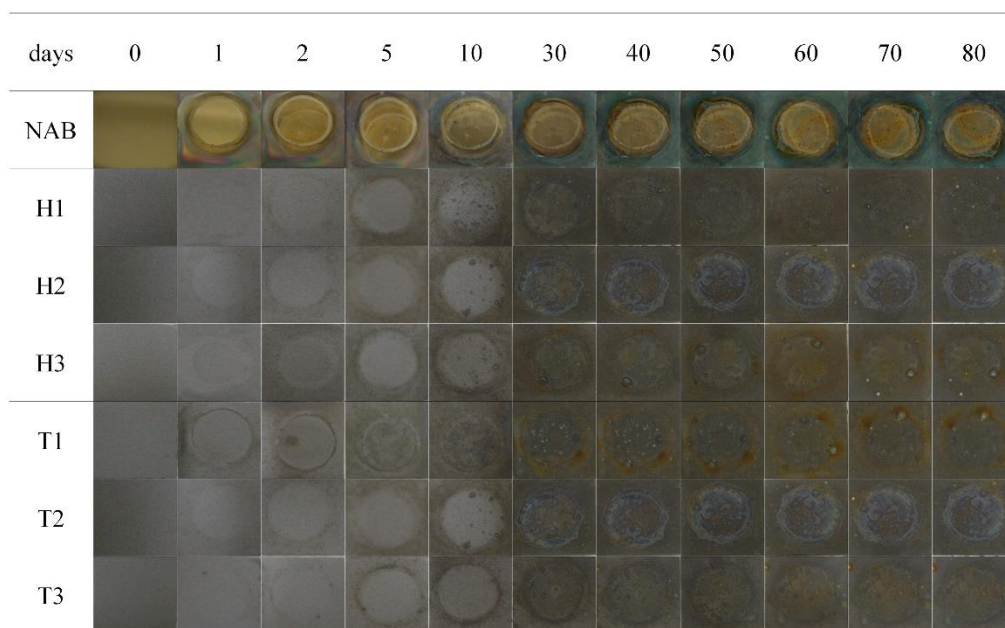


**Figure 5.** Optical microscope images of the uncoated NAB alloy and the WC-10Co-4Cr coated NAB alloys during 80-day immersion tests in a 3.5% NaCl solution.

Fig. 5 shows surface images of immersion tests in the NaCl solution along with the immersion durations. After an immersion of 10 days, the uncoated NAB alloy exhibited a perceptible change of color to green, via the formation of a passivation layer, which may be seen outside the rubber ring. Products of severe corrosion are visible as red areas around the rubber ring, indicating that iron rust has formed through breakdown of the passivation layer due to the very corrosive environment in the uncoated NAB alloy surface around the rubber ring. As previously mentioned, a suitable geometry for crevice corrosion was intentionally created by selecting a rubber ring with circular cross-section. This geometry was designed to simulate accelerated corrosion at room temperature. It was found that the uncoated NAB alloy exhibited a thick passivation layer outside the rubber ring, and a considerable amount of rust around the ring, after 80 days in the NaCl solution. On the other hand, the surfaces of the WC-Co-Cr coated NAB alloys do not show evidence of serious corrosion even after 80 days in the NaCl solution, regardless of the coating conditions. Local surfaces in contact with the rubber rings merely show a certain amount of rust under conditions of crevice corrosion.

It is observed that the degree of corrosion around the rubber ring depends on the HVOF coating conditions. The H3 specimen, coated at a longer spray distance of 260 mm, produces more corrosion products than the H1 and H2 specimens, which were processed using shorter spray distances. Variation in the hydrogen flow rate also produces differences in the degree of corrosion. The T1 specimen, coated at a hydrogen flow rate of  $55 \text{ l min}^{-1}$  shows more serious corrosion around the rubber ring. The results of the 80-day immersion tests are consistent with the conclusions derived from the polarization curves presented in Fig. 4. First, the WC-Co-Cr coated NAB alloy is superior to the uncoated NAB alloy in preventing or retarding corrosion in the NaCl solution. Secondly, WC-Co-Cr coatings processed using shorter spray distances and higher hydrogen flow rates are more effective for resisting corrosion, even in harshly corrosive environments.

#### 4. CONCLUSIONS

NAB alloy has been widely used as a casting material for screw propellers of ships operating at high torque in seawater. In order to extend the lifetime of NAB ship propellers in seawater by enhancing corrosion resistance, WC-Co-Cr coatings were thermally sprayed onto the NAB alloy under varying spray conditions, such as spray distance and hydrogen flow rate in the HVOF process. The electrochemical characteristics of the WC-Co-Cr coated NAB alloys and the uncoated NAB alloy were compared by plotting the potentiodynamic polarization curves for specimens immersed in a 3.5% NaCl solution. Actual corrosion tests of the specimens were conducted by immersing them in the NaCl solution for 80 days. Rubber rings with circular cross sections, which were devised to facilitate measuring the acceleration of corrosion in the NaCl solution, revealed differing degrees of corrosion dependent on the spray conditions. It was found that the corrosion resistance of the WC-Co-Cr coated NAB alloy exceeds that of the uncoated NAB alloy in the NaCl solution. The spray distance and hydrogen flow rate in the HVOF process have considerable influence on the anti-corrosion characteristics of WC-Co-Cr coated NAB alloys.

As a result, in this article, we introduced anti-corrosive and adherent WC-Co-Cr coatings

formed on NAB alloys by using HVOF thermal spray process. Main benefit of WC-Co-Cr coated NAB alloy component is to be repaired easily with relatively very low cost when it is corroded in seawater. NAB alloys with thermally sprayed WC-Co-Cr coatings by the HVOF process showed much better corrosion resistance than uncoated NAB alloy in a 3.5% NaCl solution. Fundamental study regarding the HVOF spray WC-Co-Cr coating as an anti-corrosive layer of NAB alloy in seawater environment was rarely conducted in the past despite of its benefits.

#### ACKNOWLEDGEMENTS

This work was partly supported by the National Research Foundation of Korea(NRF) grant funded by the Korea government(MSIT) (NRF-2017R1A2B4011380) and the Korea Institute of Energy Technology Evaluation and Planning(KETEP) grant funded by the Korea government(MOTIE) (20172010105220).

#### References

1. C.H. Tang, F.T. Cheng, H.C. Man, *Surf. Coat. Technol.*, 182 (2004) 300.
2. J.A. Wharton, R.C. Barik, G. Kear, R.J.K. Wood, K.R. Stokes, F.C. Walsh, *Corros. Sci.*, 47 (2005) 3336.
3. A. Al-Hashem, P.G. Caceres, W.T. Riad, H.M. Shalaby, *Corrosion*, 51 (1995) 331.
4. S. Sivaprasad, S. Tarafder, V.R. Ranganath, M. Tarafder, K.K. Ray, *Corros. Sci.*, 48 (2005) 1996.
5. A. Al-Hashem, W. Riad, *Mater. Charact.*, 48 (2002) 37.
6. M. Atlar, *MER-Mar. Eng. Rev.*, Sept. (2004) 64.
7. A. Edrissy, T. Perry, A.T. Alpas, *Wear*, 259 (2005) 1056.
8. S.P. Tambe, S.K. Singh, M. Patri, D. Kumar, *Prog. Org. Coat.*, 62 (2008) 382.
9. L. Zhao, M. Maurer, F. Fischer, R. Dicks, E. Lugscheider, *Wear*, 257 (2004) 41.
10. J.-Y. Kim, D.-S. Lim, S.-R. Lee, E.-S. Byun, G.-H. Lee, *J. Korean Ceram. Soc.*, 32 (1995) 1315.
11. M. Hadad, M. Hockauf, L.W. Meyer, G. Marot, J. Lesage, R. Hitzek, S. Siegmann, *Surf. Coat. Technol.*, 202 (2008) 4399.
12. J.A. Picas, M. Punset, E. Rupérez, S. Menargues, E. Martin, M.T. Baile, *Surf. Coat. Technol.*, 371 (2019) 378.
13. G. Bolelli, R. Giovanardi, L. Lusvardi, T. Manfredini, *Corros. Sci.*, 48 (2006) 3375.
14. M. Takeda, N. Morihito, R. Ebara, Y. Harada, R. Wang, M. Kido, *Mater. Trans.*, 43 (2002) 2860.
15. J.E. Cho, S.Y. Hwang, K.Y. Kim, *Surf. Coat. Technol.*, 200 (2006) 2653.
16. R. Ahmed, G. Vourlias, A. Algoburi, C. Vogiatzis, D. Chaliampalias, S. Skolianos, L.-M. Berger, S. Paul, N. H. Faisal, F.-L. Toma, N. M. Al-Anazi, M. F. A. Goosen, *J. Therm. Spray Technol.*, 27 (2018) 1579.
17. Z.-G. Ban, L.L. Shaw, *J. Therm. Spray Technol.*, 12, (2003) 112.
18. H. Wang, Q. Qiu, M. Gee, C. Hou, X. Liu, X. Song, *Mater. Des.*, 191 (2020) 108586.
19. O.P. Oladijo, B.A. Obadele, A.M. Venter, L.A. Cornish, *Afr. Corros. J.*, 2(1) (2016) 37.
20. X. Ding, D. Ke, C. Yuan, Z. Ding, X. Cheng, *Coatings*, 8(9) (2018) 307.
21. A.G. Bulnes, V.A. Fuentes, I.G. Cano, S. Dosta, *Coatings*, 10(12) (2020) 1157.
22. A. Agüero, F. Camón, J. García de Blas, J.C. del Hoyo, R. Muelas, A. Santaballa, S. Ulargui, P. Vallés, *J. Therm. Spray Technol.*, 20 (2011) 1292.
23. S. Hong, Y. Wu, Y. Zheng, B. Wang, W. Gao, G. Li, G. Ying, J. Lin, *J. Mater. Eng. Perform.*, 23(4) (2014) 1434.
24. D. Naha, S. Chatterjee, M. Ghosh, J. Dutta Majumdar, A. Majumdar, *IOSR J. Appl. Phys.*, 8(1)

(2016) 47.

25. H. Varol Özkavak, Ş. Şahin, M.F. Saraç, Z. Alkan, *Mater. Res. Express*, 6 (2019) 096554.

26. G. Padmavathi, B.N. Sarada, S.P. Shanmuganathan, R. Krishnamurthy, B.V. Padmini, *AIP Conf. Proc.*, 2317 (2021) 020013.

27. T. Varis, T. Suhonen, A. Ghabchi, A. Valarezo, S. Sampath, X. Liu, S.-P. Hannula, *J. Therm. Spray Technol.*, 23 (2014) 1009.

© 2021 The Authors. Published by ESG ([www.electrochemsci.org](http://www.electrochemsci.org)). This article is an open access article distributed under the terms and conditions of the Creative Commons Attribution license (<http://creativecommons.org/licenses/by/4.0/>).